# Extended Malus law with terahertz metallic metamaterials for sensitive detection with giant tunable quality factor

Xavier Romain,* Fadi Baida, and Philippe Boyer
*Département Optique, Institut FEMTO-ST UMR 6174, Université Bourgogne Franche-Comté, CNRS, 25030 Besançon Cedex, France*

(Received 13 January 2016; revised manuscript received 29 April 2016; published 6 July 2016)

We study a polarizer-analyzer mounting for the terahertz regime with perfectly conducting metallic polarizers made of a periodic subwavelength pattern. With a renewed Jones formalism, we analytically investigate the influence of the multiple reflections, which occur between the polarizer and the analyzer, on the transmission response. We demonstrate that this interaction leads to a modified transmission response: the extended Malus law. In addition, we show that the transmission response can be controlled by the distance between the polarizer and the analyzer. For particular setups, the mounting exhibits extremely sensitive transmission responses. This interesting feature can be employed for high-precision sensing and characterization applications. We specifically propose a general design for measuring the electro-optical response of materials in the terahertz domain allowing detection of refractive index variations as small as $10^{-5}$.

DOI: 10.1103/PhysRevB.94.045407

## I. INTRODUCTION

Unusual light phenomena, such as extraordinary optical transmission based on periodically pierced metallic films, can be observed and engineered when using subwavelength patterned materials also known as metamaterials [1–3]. Since the advent of metamaterials, the enhanced optical transmission, based on the excitation of guided mode inside subwavelength apertures, has been extensively studied in our team [4–6]. Presently, metamaterials are used for polarization applications such as in anisotropic plates [7,8], and polarization manipulation [9–11], with higher performances compared to conventional components used in visible/IR spectral domain. For the terahertz (THz) domain, natural materials do not exhibit efficient dichroism. For these frequencies, it is well known that linear polarizers are commonly obtained with frequency selective surfaces or with metallic gratings. Some papers demonstrated the polarizing properties of periodic subwavelength apertures with the use of the well-known Malus law [12–15]. Nevertheless, recent experimental results are clearly in contradiction with the output transmission predicted theoretically by this law when using subwavelength patterned metallic polarizers [16,17]. One explanation for this breakthrough involves the reflections between the plates [17].

In this paper, we report a theory of an extended Malus law for the metallic polarizer-analyzer mounting (PAM). For a specific configuration based on multiple reflections inside the PAM, we propose a principle for new ultrasensitive sensors with giant quality factors controlled by the angle between the polarizer axes. Precisely, we study a PAM as illustrated in Fig. 1, made of parallel metallic polarizers with biperiodic subwavelength grating, where each periodic cell consists of a single rectangular aperture. The angle between the polarizer and the analyzer axes is denoted by $\theta$. The periods along $x$ and $y$ axes (at $\theta = 0^\circ$) are identical and denoted by $p$. Each rectangular aperture only supports the fundamental guided mode $TE_{01}$. The linear electric polarization at the output of a polarizer is thus defined along the rectangle width axis for the working wavelengths chosen as $\lambda > \lambda_{c,TE_{01}}$. In this case, $\lambda_{c,TE_{01}} = 2a_y > p$ (subwavelength approximation), $\lambda_{c,TE_{01}}$ being the cutoff wavelength of $TE_{01}$. The higher-order modes, with cutoff wavelength $< p$, are evanescent. For this study, metal is assumed to be a perfect electric conductor at THz frequencies.

The analytical expression of the extended Malus law is deduced from a renewed Jones formalism for metallic polarizers [18,19] based on a monomode modal method [7,20–22]. We show that this extended Malus law is given by

$$I_{out} = \vec{E}_{out} \cdot \vec{E}^*_{out} = I_{in}|\alpha(\theta,\lambda,L)|^2 \cos^2\theta, \qquad (1)$$

where $*$ denotes the complex conjugate, $I_{out}$ is the output electric intensity, $\vec{E}_{out}$ is the transmitted electric field, $I_{in} = \vec{E}_{in} \cdot \vec{E}^*_{in}$, is the electric intensity incident on the polarizer. The modulation factor $\alpha$ is analytically expressed in Sec. II. Nevertheless, we highlight its dependencies on three main parameters which affect the resonance properties of the studied PAM. First, the $\theta$ dependency causes the substantial discrepancies with the well-known and classical Malus law (electric intensity proportional to square cosine of $\theta$). Besides, $\theta$ controls the quality factor of PAM resonances. Second, the coefficient $\alpha$ is an Airy-type spectrally resonant term ($\lambda$ dependency) which ensures a perfect transmission at polarizers resonances [18]. Third, we have specified in Eq. (1) the dependency of $\alpha$ on the optical path $L = n_i d$, where $n_i$ is the refractive index of the space between polarizer and analyzer separated by a distance $d$ (see Fig. 1). We will show that this parameter $L$ is linked to the multiple reflections between polarizers and controls the sensitivity of PAM resonances.

In Sec. II, we present the theoretical formalism which allows us to derive the extended Malus law given in Eq. (1). To underline the influence of the multiple reflections inside the PAM, we compare it with the one obtained with dichroic polarizers. Afterwards, we numerically investigate the PAM's transmission response to highlight the properties of the extended Malus law. Particularly, we show that high sensitivity can be obtained. In Sec. III, we take benefits of this interesting

*xavier.romain@femto-st.fr

 

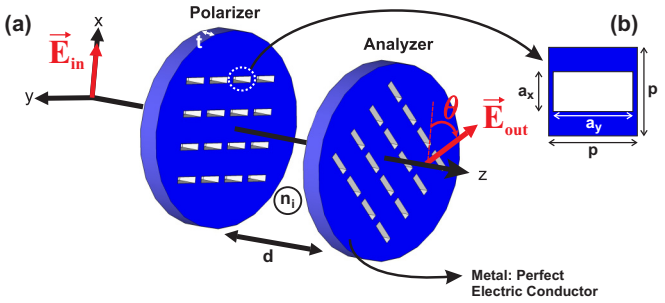


FIG. 1. (a) 3D view of the polarizer-analyzer mounting (PAM) where $d$ is the distance between polarizer and analyzer, $n_i$ is the refractive index of the space between the two metallic plates, $t$ is the plate thickness, and $\theta$ is the angular difference between polarizer and analyzer axes. (b) 2D view of the considered subwavelength pattern with $p$ the biperiodicity, and $a_x$ and $a_y$ the rectangle's width and length, respectively.

property to propose a device combining a good sensitivity, a tunable quality factor, and a high extinction ratio over a spectral broad band.

## II. TUNABLE TRANSMISSION RESPONSE OF A METALLIC POLARIZER-ANALYZER MOUNTING

### A. Theoretical framework

Our model is based on a monomode modal method [7,20–22] which considers that, only the fundamental guided mode of the rectangular apertures is excited and it propagates along the metal film thickness. It has to be noted that the formalism is also applicable to other common two-dimensional (2D) shapes such as split-ring resonators [23] and annular apertures [24], and also one-dimensional (1D) shapes such as wire grids [25]. The light passes through the PAM along the $z$ direction. We assume that working wavelengths are higher than the first Rayleigh wavelength. This means that only the 0th diffracted order in Fourier-Rayleigh expansions is propagative in homogeneous regions inside and outside the PAM. We consider a far-field approximation, where the evanescent waves are not taken into account in the spatial description of the electromagnetic fields. In other words, Fourier-Rayleigh expansions are reduced to the single propagative 0th diffracted order. This last assumption is verified especially for $L > \lambda/2$. However, evanescent diffracted orders are taken into account for the computation of the transmission and reflection Jones matrices $J_k^{T,R}$ of the $k$th polarizer ($k \in \{1,2\}$). It can be expressed as follows [18]:

$$J_k^{T,R} = \alpha_{T,R}(\lambda) J_k - \xi_{T,R} I_d, \tag{2}$$

where $I_d$ is the identity matrix, $\xi_T = 0$, and $\xi_R = 1$. The terms $\alpha_{T,R}(\lambda)$ are Fabry-Perot–type spectral resonant transmission/reflection complex coefficients for the $k$th polarizer [18]. For the whole study, the optogeometrical parameters are identical for both polarizers and they differ by their orientation only. Hence, the resonant terms $\alpha_{T,R}$ are identical for the polarizer and the analyzer. $J_1$ and $J_2$ are conventional transmission Jones matrices. $J_1$ being that of a linear polarizer oriented along the $x$ axis, and $J_2$ being that of the analyzer which is rotated from the $x$ axis by an angle $\theta$. $J_k^{T,R}$ identifies to the propagative 0th diffracted order 2×2 subblocks of the full scattering matrix for each polarizer. Hence, the scattering propagation algorithm [26] is used to analytically compute the transmission Jones matrix of the PAM $J_{\text{PAM}}^T$. After extensive calculations, we obtain

$$J_{\text{PAM}}^T = \alpha(\theta,\lambda,L) J_2 J_1. \tag{3}$$

We focus on the transmitted output intensity. Then, the expression of the reflection Jones matrix of the PAM is not given in this paper. The extended Malus law given in Eq. (1) is directly derived from Eq. (3), where the term $\alpha$ is expressed as

$$\alpha(\theta,\lambda,L) = \frac{\alpha_T^2(\lambda) u}{\gamma - u^2[1-\alpha_R(\lambda)]^2} \tag{4}$$

with

$$\gamma = \frac{1 - u^2\left[1 - \alpha_R^2(\lambda)\sin^2\theta\right]}{1-u^2}, \tag{5}$$

where $u = \exp(ik_0 L)$, is the propagation term between the polarizer and the analyzer, with $k_0 = 2\pi/\lambda$. It is important to notice that in our study, the extended Malus law is evaluated at spectral resonances of $\alpha$ (maxima of $|\alpha|$). The $\theta$ dependency of $\alpha$ clearly appears in the expression of $\gamma$ with $\sin^2\theta$ in Eq. (5). This term is multiplied by $\alpha_R^2(\lambda)$, which implies that the multiple reflections occurring between the two polarizers are directly linked to the transmission response and provoke the important discrepancies with the classical Malus law. Moreover, the term $u^2$ in the numerator of $\gamma$ means that the optical path $L$ controls the influence of the multiple reflections on the extended Malus law variation.

It has to be noted that a device with similar polarization properties called Malus Fabry-Perot interferometer was theoretically investigated in 1999 by Vallet *et al.* [27]. This device consisted of a Fabry-Perot interferometer inside a PAM (without spectral resonances of polarizing plates) made of crossed polarization beam splitters. The two mirrors of that device produce similar multiple reflections to the ones generated by the metallic polarizers in our structure. However, the behaviors of these two kinds of polarizing resonators are different. For the Malus Fabry-Perot interferometer [27], the Fabry-Perot resonances and polarization effects are independent. For our structure, the metallic plates play the role of both polarizers and mirrors. At resonance, only the waves polarized along the rectangle's length axis are reflected inside the PAM. The Fabry-Perot–type resonances between polarizers and polarization effects are closely linked, and this is exploited to perform the efficient application proposed in Sec. III.

Our formalism also allows us to compute the classical Malus law obtained with dichroic polarizing plates. We first give the general expression of the reflection Jones matrix of the $k$th polarizer oriented along the $x$ axis:

$$J_k^R = \begin{pmatrix} \alpha_R - 1 & 0 \\ 0 & \beta \end{pmatrix}, \tag{6}$$

where $\beta$ is the reflection coefficient of one polarizer along the rectangle length axis, calculated in accordance with

the absorption along this axis only. For metallic polarizers, $\beta = -1$ (no absorption), Eq. (6) is identical to Eq. (2) for $k = 1$. For dichroic polarizer, $\beta = 0$ (total absorption along the rectangle length axis) which means that the multiple reflections in the PAM are reduced to the ones oriented along the rectangle width axis (term $\alpha_R - 1$ in $J_k^R$). These reflections are weak for most of the natural dichroic plates. This leads to the expression $\alpha_d$ for $\alpha$ of Eq. (1) in the case of the classical Malus law, when the multiple reflections are not neglected ($\beta = 0$ and $\alpha_R \approx 1$ with $\alpha_R \neq 1$):

$$\alpha_d(\theta,\lambda,L) = \frac{\alpha_T^2(\lambda)u}{1 - u^2[1-\alpha_R(\lambda)]^2\cos^2\theta} \quad \underset{\alpha_R\to 1}{\longrightarrow} \alpha_T^2(\lambda)u. \tag{7}$$

This equation highlights the discrepancies between the factor $\alpha_d$ found for commonly used dichroic polarizers and the modulation factor $\alpha$ previously obtained for metallic polarizer [Eqs. (4) and (5)]. We see that $\alpha_d$ is dependent on $\theta$, but the factor $u^2[1-\alpha_R(\lambda)]^2$ relating to the multiple reflections may be neglected for the special case of highly absorbing dichroic polarizers ($\alpha_R \to 1$). On the contrary, the term $u^2[1-\alpha_R^2(\lambda)\sin^2\theta]$ cannot be neglected in Eq. (5) for the case of metallic polarizers. Indeed, we know that $\alpha_R \approx 1$ when $|\alpha_T| = 1$ due to the energy balance criterion: $|\alpha_T^2 - (\alpha_R - 1)^2| = 1$ (see Fig. 3 in [18]). Consequently and contrary to the extended Malus law for metallic polarizers, we can assume that $\alpha_d$ is independent of $\theta$, as it is well known for dichroic polarizers. The extended Malus law takes the form of the classical one which corresponds to the single pass propagation through the PAM as shown in Eq. (7).

### B. Numerical results

We propose a numerical investigation of the PAM's transmission depicted in Fig. 1. We focus on the influence of the optical path $L$. The rectangles of the polarizer and the analyzer are identical and its dimensions are given by $a_y/p = 0.9$ and $a_x/p = 0.45$. These values are chosen such that the radiative losses of the apertures are maximized (broadband transmission). Besides, the $a_x/p$ value is set to ensure that only the fundamental mode can propagate in apertures at wavelengths located above the Rayleigh anomaly (monomode regime). In other words, the cutoff wavelength of the second cavity mode is smaller than the first Rayleigh wavelength. The thickness of the polarizer and the analyzer is set to $t/p = 1$. In this section, we consider that the apertures and homogeneous regions are filled with air. For all the results, we compute the normalized transmission coefficient: $I_{\text{out}}/I_{\text{in}}$.

We first calculate the transmitted electric intensity spectrum as a function of the distance $L/p$ for $\theta = 0^\circ$ ($I_{\text{out}} = |\alpha|^2$) as shown in Fig. 2, in order to reveal the spectral resonances of $\alpha$ supported by the whole structure. The resonance at $\lambda/p = 1.434$ (blue vertical line) corresponds to the first harmonic of the Fabry-Perot resonance ($\text{FP}_A$) of the fundamental mode guided inside the rectangular apertures along the metal thickness. The resonance at $\lambda/p = 1.69$ (red vertical line) corresponds to the cut-off of the same mode ($CO$). Both resonances correspond to the transmission resonances of one metallic polarizer: $|\alpha_T(\lambda)| = 1$. The different oblique

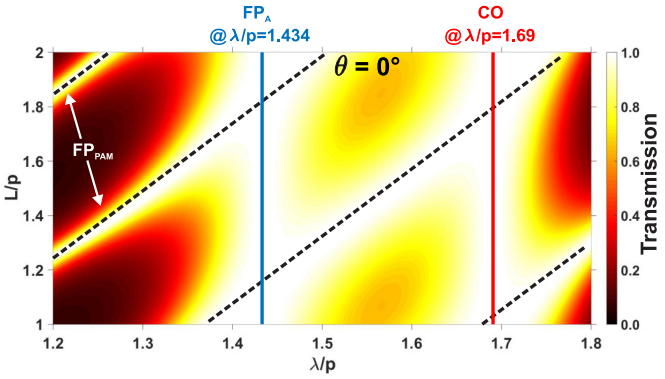


FIG. 2. Normalized transmitted electric intensity spectra of the PAM versus $L/p$ for $\theta = 0^\circ$. The parameters are $a_x/p = 0.45$, $a_y/p = 0.9$, and $t/p = 1.0$. Vertical lines show resonances of $|\alpha|$ ($I_{\text{out}} = 1$). The resonance at $\lambda/p = 1.434$ is related to the first harmonic of the Fabry-Perot resonance of the fundamental mode guided inside the rectangular apertures ($\text{FP}_A$). The other resonance at $\lambda/p = 1.69$ corresponds to the cutoff of the same mode ($CO$). The $\text{FP}_{\text{PAM}}$ branches (oblique dashed lines) denotes Fabry-Perot interferences located between the polarizer and the analyzer.

branches ($\text{FP}_{\text{PAM}}$ in oblique dashed line) are the Fabry-Perot resonances resulting from the multiple reflections between the two polarizers. The $\text{FP}_A$ and $CO$ resonances ensure a total transmission for any value of $L/p$. Then, we restrict our analysis to the transmission at $\text{FP}_A$ and $CO$ resonances related to each polarizer.

Figure 3(a) shows the transmission spectra as a function of $\theta$ for $L/p = 1$. It reveals that resonance wavelength values are affected by the variation of $\theta$ (dashed lines). Figure 3(b) shows the transmission at the resonance wavelengths plotted as solid lines in Fig. 3(a), for $\theta = 0^\circ$. It is compared with the classical Malus law (dashed black line) for which the half-width half-maximum (HWHM) is equal to $\pi/4$. The observed discrepancies confirm the important contribution of the multiple reflections between the polarizer and the analyzer. The results obtained with our analytical model are in good agreement with results obtained with homemade FDTD code [4]. The FDTD simulations were done with a uniform spatial mesh of $p/200$ along the $x$, $y$, and $z$ axes, and a temporal resolution respecting the stability criterion.

In Fig. 4(a), we choose $\lambda/p = 1.434$ ($\text{FP}_A$ resonance) and we plot the transmission as a function of $\theta$ and $L/p$. As mentioned in Sec. II A, the optical path $L/p$ is an important parameter that will allow us to tune the PAM transmission. We distinguish two contrasting cases:

(1) When $u^2 = 1$ which is equivalent to $L = m\lambda/2$ where $m$ is a natural integer, we observe an infinitely narrow angle Malus law where HWHM $\ll \pi/4$. Precisely, the transmitted electric intensity drops to 0 for this particular value of $L/p$ when $\theta \neq 0^\circ$. Indeed, this is explained by the fact that the term $\gamma$ in Eq. (5) diverges when $\theta \neq 0^\circ$. For $\theta = 0^\circ$, we clearly see that $\gamma = 1$. This implies that $\alpha = \alpha_T^2(\lambda)/\alpha_R^2(\lambda)$ approximately equals to 1 at maxima of $\alpha_T$ ($I_{\text{out}} \approx 1$). For clarity, the Malus law is shown in Fig. 4(b) for $L/p = 1.435$ (green line) and not exactly at $L/p = 1.434$ ($u^2 = 1$ for $m = 2$) for which the

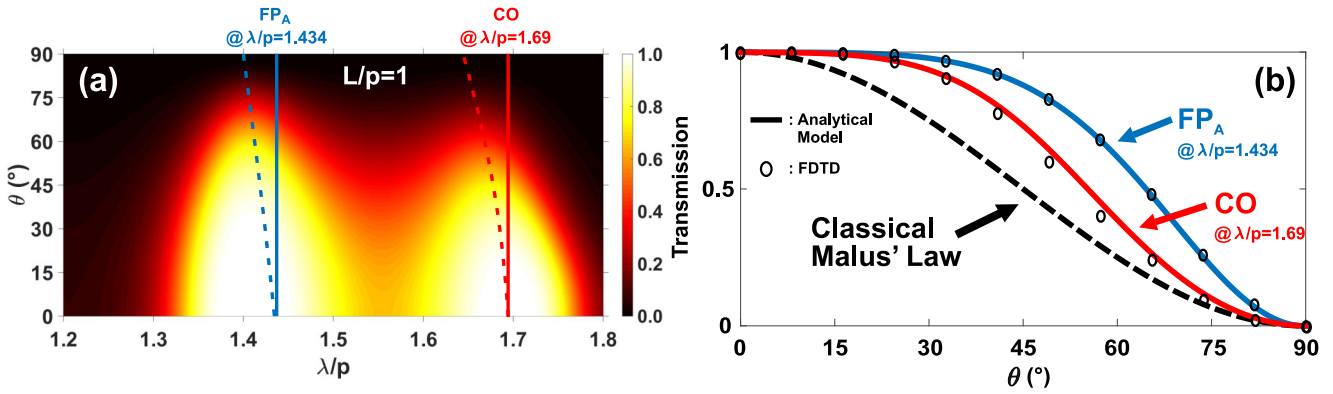


FIG. 3. (a) Normalized transmission spectra versus $\theta$ for $L/p = 1$ (see Fig. 2 for other parameters). The curved dashed lines represent the trajectories of the resonance of $\alpha$ ($|\alpha| = 1$). (b) Normalized transmission computed for fixed values of $\lambda/p$ [blue and red vertical solid lines in (a)] and compared with the classical one (dashed black line).

transmission results in a Kronecker function:

$$\alpha(\theta) = \delta_{\theta,0}. \tag{8}$$

(2) When $u^2 = -1$, which is equivalent to $L = \lambda/4 + m'\lambda/2$ where $m'$ is a natural integer, we observe broad angle Malus law. The transmitted electric intensity remains high for a wide range of $\theta$. The transmission as a function of $\theta$ is shown in Fig. 4(b) (purple line) for $L/p = 1.793$ ($u^2 = -1$ for $m' = 2$). Such a transmission can be seen as a complementary Airy-type function (HWHM $> \pi/4$) with a unity value plateau for small $\theta$. The following equation gives the simple expression of $\alpha$ for the purple line in Fig. 4(b), assuming that $\alpha_R = 1$ (the computed value being exactly equal to $1.0077 + i0.1307$):

$$\alpha(\theta,\lambda) = i(-1)^{m'} \frac{\alpha_T^2(\lambda)}{1 - \frac{1}{2}\sin^2\theta}. \tag{9}$$

Consequently, both narrow and broad angle Malus law can be achieved by tuning $L$.

## III. APPLICATION TO DESIGN ULTRASENSISTIVE THZ DETECTORS WITH GIANT AND TUNABLE $Q$

Taking advantage of an infinitely narrow angle Malus law shown in the previous section for particular values of $L$, we present the principle of a spectrally sensitive system in the THz domain with a tunable quality factor. Such a system can be used for many applications, like for temperature or pressure sensors, or characterization of an electro-optical (EO) material. We now assume that the region sandwiched between the polarizers with $\theta \neq 0°$ is filled with an isotropic, homogeneous, and transparent EO material [see Fig. 5(b)]. It is interesting to remark that the two metallic polarizers also play the role of electrodes allowing to tune the refractive index $n_i(V)$ of the EO material. For this study, the value of the distance $d$, corresponding to the EO material's thickness is fixed, so that $L$ varies only with its refractive index $n_i$. The dimensions are $p = 200\ \mu$m, $a_x = 90\ \mu$m, $a_y = 180\ \mu$m, $t = 200\ \mu$m, and $d = 200\ \mu$m.

Figure 5(a) shows the transmitted electric intensity spectrum vary with $n_i$. Contrary to the intensity spectra plotted in Fig. 2 where $\theta = 0°$, oblique and very narrow dark branches appear in transmission bands when $\theta \neq 0°$. They correspond to transmission dips satisfying $n_i = m\lambda/(2d)$ ($u^2 = 1$). In order to match the refractive index range for most of the materials in the THz domain ($n_i$ approximately between 3 and 4 [28]), we consider the branch $m = 4$. We also observe that the device can be adapted to any range of refractive index values by considering the appropriate value of $m$. The sensitivity $S$,

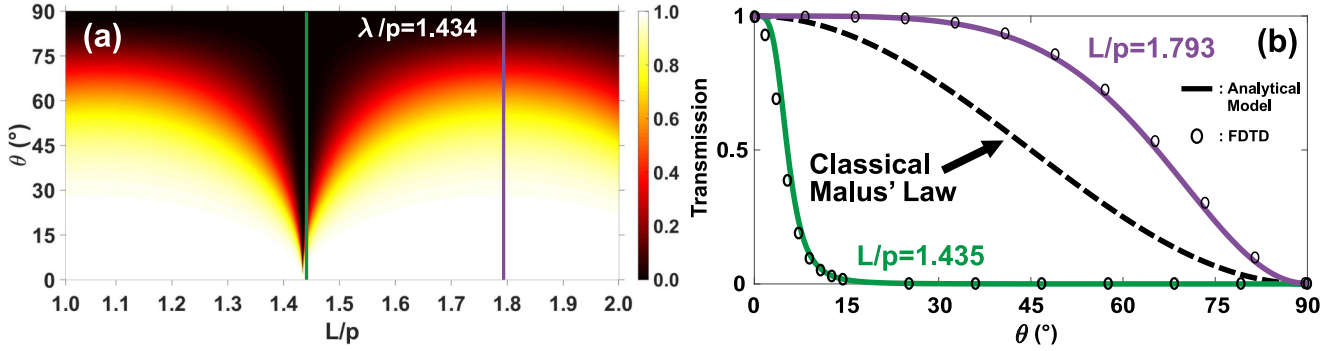


FIG. 4. (a) Normalized transmitted intensity versus $L/p$ and $\theta$ for $\lambda/p = 1.434$ (see Fig. 2 for other parameters). (b) Normalized transmission computed for fixed values of $L/p$ [green and purple vertical dashed lines in (a)] by comparison with the classical one (dashed black line).

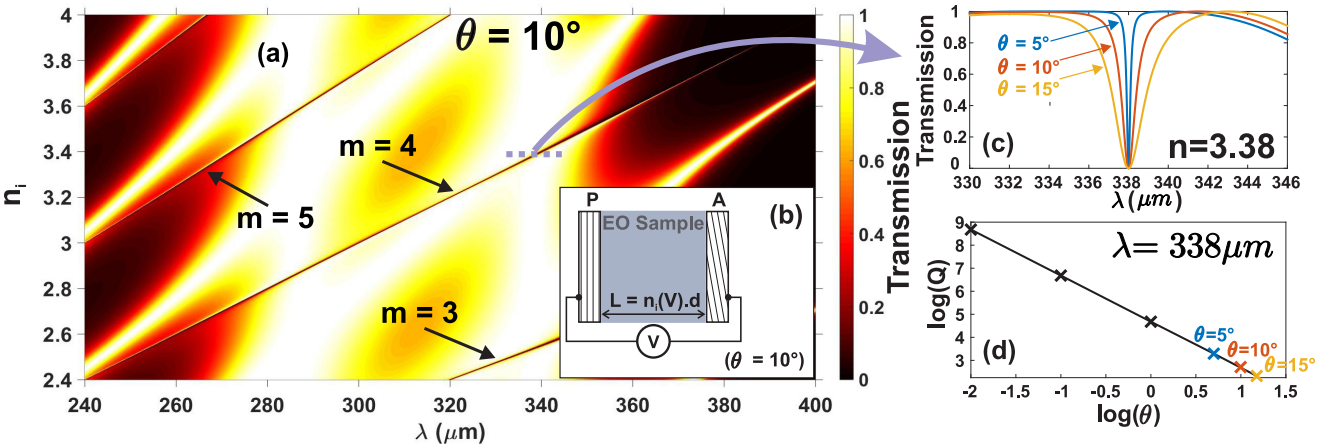


FIG. 5. (a) Normalized transmitted intensity spectrum vs the refractive index $n_i$, for $\theta = 10^\circ$. The parameters are $p = 100\ \mu$m, $a_x = 45\ \mu$m, $a_y = 90\ \mu$m, $t = 100\ \mu$m, and $d = 100\ \mu$m. The dark branches correspond to narrow transmission dips when $L = m\lambda/2$. (b) Scheme of the general principle to characterize electro-optical material responses. P: polarizer (first electrode), A: analyzer (second electrode), V: applied dc voltage, d: EO material thickness, and $\boldsymbol{n_i(V)}$: refractive index of the electro-optical sample. (c) Normalized transmission dips for different values of $\theta$ in degrees, at $n_i = 3.38$. (d) Quality factor $Q$ as a function of $\theta$ at $n_i = 3.38$.

associated to the dark branches in our case, is

$$S = \frac{\Delta\lambda}{\Delta n_i} = \frac{2d}{m}, \quad \forall\, \theta \neq 0^\circ. \tag{10}$$

For $m = 4$, we have $S = 100\ \mu$m/refractive index unit (RIU). We point out that it is possible to improve the sensitivity by increasing the thickness $d$ (tradeoff between the compactness and the sensitivity).

Figure 5(c) shows the intensity spectra for $\lambda$ close to 338 $\mu$m ($\lambda/p = 1.69$) for different values of $\theta$ at $n_i = 3.38$, which is close to the gallium phosphide (GaP) refractive index in the THz domain ($n_i \simeq n_{\text{GaP}} = 3.34$, see [28]). The dips have high extinction ratios in transmission bands, and the sensitivity is not affected by $\theta$. However, the quality factor $Q$, or in other words, the width of the transmission dips, can be controlled by adjusting $\theta$, in accordance with results presented in Fig. 4. Figure 5(d) shows the variation of the quality factor $Q$ as a function of $\theta$ (for $n_i = 3.38$ at $\lambda = 338\ \mu$m). The quality factor theoretically diverges when $\theta$ tends to 0°, and the linearity of the curve allows us to write

$$Q = \frac{mA}{\theta^B}, \quad \forall\, \theta \neq 0^\circ, \tag{11}$$

where $A$ and $B$ are two empirical and positive parameters, and $\theta$ is expressed in degree. From Fig. 5(d), we deduce $B = 2$, and $A = 1.25\times10^4$ degrees$^2$, for $m = 4$.

Finally, we are interested in finding a suitable value of $\theta$ to obtain a quality factor matching the resolution of THz spectrometers under the Rayleigh criterion. Hence, we deduce the minimum variation of the refractive index $(\Delta n_i)_{\min}$ which can be detected by the device. Heterodyne detectors in THz domain offer spectral resolution [29] ($R = \Delta\lambda/\lambda$) equal to $3.3\times10^{-6}$. Thus, according to Eq. (11), to reach $Q = 1/R = 3\times10^5$, $\theta$ must be equal to 0.4° at $n_i = 3.38$ and $\lambda = 338\ \mu$m. With such a quality factor, we derive from Eq. (10) that $(\Delta n_i)_{\min} = \lambda/(S.Q) = 1.1\times10^{-5}$.

Consequently, we have designed a very efficient system for THz applications ($S = 100\ \mu$m/RIU, $Q = 3.10^5$). Ranjan Singh *et al.* [30] have experimentally proposed a metasurface reaching $S = 57\ \mu$m/RIU and $Q = 28$. We have to keep in mind that our numerical results are obtained from a theory which assumes rigorously identical apertures and infinite periodicity of the metallic polarizers, in addition to a perfect parallelism between the polarizer and the analyzer. We also assume an isotropic and lossless EO material. Breaking these assumptions may affect the performances of the proposed system.

## IV. CONCLUSION

In summary, we have given an analytical formalism of an extended Malus law with metallic polarizers for the terahertz regime. Our theoretical investigation highlights the important discrepancies with the classical Malus law. This is due to the $\theta$ dependency of the modulation factor as well as the multiple reflections inside the PAM which are tunable through the optical path $L$. Indeed, for specific values of $L$ one can obtain broad angle or narrow angle Malus law. Then, we designed a structure with high sensitivity and high-quality factor for characterizing the EO response of terahertz EO material based on an extremely narrow angle Malus law. This analytical model of a two-layer stack of subwavelength structures provide new theoretical insights into the interactions between polarizing metamaterials. This simple structure can be seen as the basic component for multilayered and more complex structures. In future works, we will use our analytical model as a platform to propose other applications such as high-efficiency polarization conversion, high-$Q$ filtering, and ultrasensitive polarimetry.

## ACKNOWLEDGMENTS

This project has been performed in cooperation with the Labex ACTION program (Contract No. ANR-11-LABX-0001-01). The authors would like to thank T. Kuriakose and A. Shaw for their helpful advice.

## APPENDIX A: JONES MATRICES FOR THE METALLIC POLARIZERS

From the monomode modal method [22], we extract the 2×2 subblocks for the 0th diffracted order of the scattering matrix of a metallic polarizer. This reduced matrix, denoted by $S$, is expressed as

$$S = \begin{pmatrix} J^T & J^R \\ J^R & J^T \end{pmatrix} \quad \text{with } J^{T,R} = f_{T,R}\begin{pmatrix} \tilde{g}_{0,x}\tilde{g}^*_{0,x} & \tilde{g}_{0,x}\tilde{g}^*_{0,y} \\ \tilde{g}_{0,y}\tilde{g}^*_{0,x} & \tilde{g}_{0,y}\tilde{g}^*_{0,y} \end{pmatrix} - \xi_{T,R}\begin{pmatrix} 1 & 0 \\ 0 & 1 \end{pmatrix}, \tag{A1}$$

where $J^T$ and $J^R$ are the Jones matrices for the transmission and reflection, respectively. The terms $f_{T,R}$ are Airy-type spectral resonant factors in transmission and reflection [18]. $\xi^T = 0$ and $\xi^R = 1$. The coefficients $\tilde{g}_{0,x}$ and $\tilde{g}_{0,y}$ are the overlap integral between the fundamental cavity mode $TE_{01}$ and the 0th order Floquet modes, polarized along $x$ and $y$ axis, respectively. For a normal incidence and for rectangular apertures, their expressions are given by

$$\tilde{g}_{0,x} = \frac{2}{\pi}\sqrt{\frac{2a_x a_y}{d_x d_y}}\cos\theta \quad \text{and} \quad \tilde{g}_{0,y} = \frac{2}{\pi}\sqrt{\frac{2a_x a_y}{d_x d_y}}\sin\theta. \tag{A2}$$

Substituting Eq. (A2) in (A1) leads to Eq. (2) where $\alpha_{T,R}$ are expressed as

$$\alpha_{T,R} = f_{T,R}\left|\frac{2}{\pi}\sqrt{\frac{2a_x a_y}{d_x d_y}}\right|^2. \tag{A3}$$

## APPENDIX B: EXTENDED MALUS LAW DEMONSTRATION

In this appendix, we give the main steps to derive the analytical expressions of the extended Malus law given by Eq. (1), from the ones of the Jones matrices for metallic polarizer and analyzer given by Eq. (2). The PAM is seen as a three-layer system. The first and the third layers are the polarizer and the analyzer, respectively. The reduced $S$ matrix for each polarizer is expressed as

$$S_k = \begin{pmatrix} J^T_k & J^R_k \\ J^R_k & J^T_k \end{pmatrix}, \quad k \in \{1,2\}. \tag{B1}$$

The matrices $J^{T,R}_k$ are given by Eq. (2). The second layer corresponds to the homogeneous region between both polarizers. Its reduced $S$ matrix is given by

$$S_{\text{hom}} = \begin{pmatrix} J_{\text{hom}} & 0 \\ 0 & J_{\text{hom}} \end{pmatrix} \quad \text{with } J_{\text{hom}} = \begin{pmatrix} u & 0 \\ 0 & u \end{pmatrix}, \tag{B2}$$

where $u = \exp(ik_0 L)$, is the propagation term between polarizers.

The theoretical approach consists in applying the scattering matrix propagation algorithm [26] ($S$ algorithm) on the reduced $S$ matrices twice. The operator related to the $S$ algorithm is denoted as $\otimes$. The first iteration of $S$ algorithm is

$$S' = S_1 \otimes S_{\text{hom}} = \begin{pmatrix} uJ^T_1 & u^2 J^R_1 \\ J^R_1 & uJ^T_1 \end{pmatrix}, \tag{B3}$$

where $S'$ is the $S$ matrix of the system composed of the polarizer and the homogeneous region. Then, the reduced scattering matrix of the PAM, $S_{\text{PAM}}$, is obtained by the second iteration of the $S$ algorithm applied on $S'$ and $S_2$:

$$S_{\text{PAM}} = S' \otimes S_2 = \begin{pmatrix} J^T_{\text{PAM}} & J^R_{\text{PAM}} \\ J^R_{\text{PAM}} & J^T_{\text{PAM}} \end{pmatrix}, \tag{B4}$$

where $J^{T,R}_{\text{PAM}}$ are transmission and reflection Jones matrix of the PAM. The expression of $J^R_{\text{PAM}}$ is not given in this paper since it is not useful to express the extended Malus law. The matrix $J^T_{\text{PAM}}$ is

$$J^T_{\text{PAM}} = uJ^T_2\left[I_d - u^2 J^R_1 J^R_2\right]^{-1} J^T_1, \tag{B5}$$

where the inversion of $I_d - u^2 J^R_1 J^R_2$, after substituting expression of $J^R_1$ and $J^R_2$ given by (2), is

$$\left[I_d - u^2 J^R_1 J^R_2\right]^{-1} = \frac{1}{D}\begin{pmatrix} 1-u^2(1-\alpha_R\sin^2\theta) & -u^2(1-\alpha_R)\alpha_R\cos\theta\sin\theta \\ -u^2\alpha_R\cos\theta\sin\theta & 1-u^2(1-\alpha_R)(1-\alpha_R\cos^2\theta) \end{pmatrix} \tag{B6}$$

with

$$D = 1 + u^2(u^2-1)(1-\alpha_R)\left(\alpha^2_R\sin^2\theta - 1\right). \tag{B7}$$

Substituting Eqs. (B6) and (B7) in (B5) leads to Eq. (3).


[1] V. G. Veselago, Usp. Fiz. Nauk **92**, 517 (1964) [Sov. Phys. Usp. **10**, 509 (1968)].
[2] J. B. Pendry, Phys. Rev. Lett. **85**, 3966 (2000).
[3] T. W. Ebbesen, H. J. Lezec, H. F. Ghaemi, T. Thio, and P. A. Wolff, Nature (London) **391**, 667 (1998).
[4] F. I. Baida and D. Van Labeke, Opt. Commun. **209**, 17 (2002).
[5] A. Moreau, G. Granet, F. Baida, and D. Van Labeke, Opt. Express **11**, 1131 (2003).
[6] Y. Poujet, J. Salvi, and F. I. Baida, Opt. Lett. **32**, 2942 (2007).
[7] F. I. Baida, M. Boutria, R. Oussaid, and D. Van Labeke, Phys. Rev. B **84**, 035107 (2011).
[8] J. Dahdah, J. Hoblos, and F. I. Baida, IEEE Photon. J. **4**, 87 (2012).
[9] N. K. Grady, J. E. Heyes, D. R. Chowdhury, Y. Zeng, M. T. Reiten, A. K. Azad, A. J. Taylor, D. A. R. Dalvit, and H.-T. Chen, Science **340**, 1304 (2013).
[10] B. Shen, P. Wang, R. Polson, and R. Menon, Optica **1**, 356 (2014).
[11] C. Pfeiffer and A. Grbic, Phys. Rev. Applied **2**, 044012 (2014).
[12] R. Gordon, A. G. Brolo, A. McKinnon, A. Rajora, B. Leathem, and K. L. Kavanagh, Phys. Rev. Lett. **92**, 037401 (2004).
[13] A. Degiron, H. Lezec, N. Yamamoto, and T. Ebbesen, Opt. Commun. **239**, 61 (2004).
[14] M. Sarrazin and J.-P. Vigneron, Opt. Commun. **240**, 89 (2004).
[15] J. R. DiMaio and J. Ballato, Opt. Express **14**, 2380 (2006).

[16] C. Huang, Q. Wang, X. Yin, Y. Zhang, J. Li, and Y. Zhu, Adv. Opt. Mater. **2**, 723 (2014).
[17] C. Zhang, C. Pfeiffer, T. Jang, V. Ray, A. Grbic, and L. J. Guo, in *CLEO: 2015* (Optical Society of America, Washington, DC, 2015), p. JTu5A.96.
[18] P. Boyer, J. Opt. Soc. Am. A **31**, 1226 (2014).
[19] X. Romain, F. I. Baida, and P. Boyer, in *Proceedings of the 9th International Congress on Advanced Electromagnetic Materials in Microwaves and Optics (METAMATERIALS)* (IEEE, New York, 2015), pp. 478–480.
[20] P. Lalanne, J. P. Hugonin, S. Astilean, M. Palamaru, and K. D. Mller, J. Opt. A: Pure Appl. Opt. **2**, 48 (2000).
[21] L. Martin-Moreno, F. J. Garcia-Vidal, H. J. Lezec, K. M. Pellerin, T. Thio, J. B. Pendry, and T. W. Ebbesen, Phys. Rev. Lett. **86**, 1114 (2001).
[22] P. Boyer and D. Van Labeke, J. Opt. Soc. Am. A **29**, 1659 (2012).
[23] D. R. Smith, W. J. Padilla, D. C. Vier, S. C. Nemat-Nasser, and S. Schultz, Phys. Rev. Lett. **84**, 4184 (2000).
[24] F. I. Baida and D. Van Labeke, Phys. Rev. B **67**, 155314 (2003).
[25] I. Yamada, K. Takano, M. Hangyo, M. Saito, and W. Watanabe, Opt. Lett. **34**, 274 (2009).
[26] L. Li, J. Opt. Soc. Am. A **13**, 1024 (1996).
[27] M. Vallet, F. Bretenaker, A. Le Floch, R. Le Naour, and M. Oger, Opt. Commun. **168**, 423 (1999).
[28] Q. Wu and X.-C. Zhang, IEEE J. Sel. Top. Quantum Electron. **2**, 693 (1996).
[29] J.-L. Coutaz, *Optoelectronique Terahertz* (EDP Sciences, Paris, 2008).
[30] R. Singh, W. Cao, I. Al-Naib, L. Cong, W. Withayachumnankul, and W. Zhang, Appl. Phys. Lett. **105**, 171101 (2014).